Application of the Bruyères Jeukenne-Lejeune-Mahaux model potential to composite nuclei with a single-folding approach

D. Y. Pang,* Y. L. Ye, and F. R. Xu

School of Physics and State Key Laboratory of Nuclear Physics and Technology, Peking University, Beijing, China, 100871

(Received 28 February 2011; revised manuscript received 9 May 2011; published 30 June 2011)

A single-folding (SF) model analysis has been performed for α and deuteron elastic scattering from ^{58}Ni, ^{90}Zr, ^{116}Sn, and ^{208}Pb at incident energies between 10 and 100 MeV/nucleon with the Lane-consistent Bruyères Jeukenne-Lejeune-Mahaux model nucleon-nucleus potential. The energy dependence of a set of only three potential parameters was derived, and the resulting global optical model potentials were found to account well for α and deuteron elastic scattering within their studied energy ranges. The energy dependence of a real potential form factor is found to be important for describing α-nucleus scattering within large energy ranges. Corrections due to the compositeness of projectiles to the SF potentials were studied and were compared with theoretical estimations through the renormalization factor. Systematic differences in renormalization factors between α particles and deuterons were observed.

DOI: 10.1103/PhysRevC.83.064619 PACS number(s): 24.10.Ht, 25.10.+s, 25.45.−z, 25.55.Ci

I. INTRODUCTION

One of the major tasks for nuclear physics is to understand the properties of composite nuclei from the interactions between their constituent nucleons. Microscopic or semimicroscopic nucleus-nucleus optical model potentials (OMPs), which combine nucleon-nucleon or nucleon-nucleus interactions and nuclear structure information by folding models, are the most studied quantities for this purpose [1–3]. Problems in this subject involve nonlocality of optical potentials, Pauli principle, and three-body effects, which are essential parts of nuclear physics.

For the first approximation, the OMP of a projectile-target system can be expressed with the single-folding (SF) model [1,4],

$$U(R) = \int U_{\mathrm{NT}}(|\boldsymbol{R} + \boldsymbol{r}|)\rho_N(r)\, d\boldsymbol{r}, \tag{1}$$

where $\rho_N(r)$ is the nucleon (proton and/or neutron) density distribution of the projectile at $\boldsymbol{r}$ with respect to its center of mass (c.m.), $U_{\mathrm{NT}}(|\boldsymbol{R} + \boldsymbol{r}|)$ is the nucleon-target OMP evaluated at $|\boldsymbol{R} + \boldsymbol{r}|$ from the c.m. of the target nucleus, and $\boldsymbol{R}$ is the vector from the c.m. of the target to that of the projectile. U_{NT} is the interaction between a *free* nucleon with a target nucleus. When applying SF model potentials to composite nuclei, corrections due to compositeness of projectiles were found to be necessary. These corrections can largely be represented by renormalization of the SF potentials. Many studies have shown that real SF potentials have to be reduced, for example, around 10% for deuteron [5,6] and around 20% for ^{3}He and α particles [4,7], with respect to their phenomenological counterparts. Theoretically, these reductions can be attributed to internal motions of the constituent nucleons, the three-body effects, and the Pauli principle [4] or to nonlocality of optical model potentials and finite sizes of projectiles [8]. However, systematic studies of corrections to the imaginary SF potentials and to the real SF potentials within sufficiently large energy ranges are scarce. In this paper, we investigate this problem by analyzing α-particle elastic scattering from ^{58}Ni, ^{90}Zr, ^{116}Sn, and ^{208}Pb at incident energies between 40 and 386 MeV. Results of Ref. [4] show that, at higher energies, where effects of the Pauli principle can be neglected, it is the effect of internal motions of constituent nucleons that is mainly responsible for the reduction of SF potentials. Because of the much smaller binding energy of the deuteron, corrections for the deuteron-nucleus SF potentials are expected to be different from those for the α-nucleus potentials. To make the comparison, we analyze elastic scattering of deuterons from ^{58}Ni, ^{90}Zr, and ^{208}Pb at incident energies from 20 to 200 MeV in the same manner.

This paper was also motivated by our quest for a systematic α-nucleus OMP. Numerous studies have been devoted to α-nucleus scattering [8–17], but satisfactory global OMPs of an α particle within sufficiently large energy and target mass ranges have not been reported. Recently, at a low-energy region, the improved semimicroscopic global α-nucleus optical potentials [18] by Demetriou *et al.* were reviewed and were extended to a target mass from around 50 to 120 and incident energies from around 13 to 50 MeV. These results were elaborated on in Ref. [19] by Avrigeanu *et al.* in which a regional optical potential set was derived and was checked against α-nucleus scattering and (α, p), (α, n), and (α, γ) reactions. At a higher-energy region, Nolte *et al.* derived a global α potential for incident energies higher than 80 MeV [20] in which energy dependence of geometry parameters, namely, the radius and diffuseness parameters of Woods-Saxon form factors, were not taken into account. In this paper, we will show that an energy dependence of these parameters is needed if a global or regional OMP for an α particle is to be derived within sufficiently large energy ranges.

Phenomenological systematic nucleon-nucleus potentials are usually used in single-folding model calculations [21]. However, energy dependence of geometry parameters in systematic nucleon potentials were usually ignored [22,23].

*dypang@pku.edu.cn

These potentials, when applied in SF model calculations, will not be able to give a good account of the α-nucleus scattering over sufficiently large energy ranges. Thus, the systematic nucleon-nucleus OMP with the Jeukenne-Lejeune-Mahaux (JLM) + Bruyères (JLMB) model [24,25], which have finite-range parameters naturally built in, which allow control of the form factor of the folding-model potentials, is very suitable in SF model analysis of α-nucleus scattering. Compared to the original JLM model [26,27], Lane consistency is improved in the JLMB model, which is important for $N \neq Z$ nuclei. Systematics of normalization factors of nucleon potentials were derived in the JLMB model, which gave a good account of nucleon elastic scattering and reaction cross sections. The ability of describing free nucleon interactions with target nuclei for nucleon-nucleus potentials is important in studies of compositeness of projectiles with a SF model.

Only three parameters, namely, the finite-range parameter and renormalization factors of the real and imaginary SF potentials (see Sec. II), were used in this paper. We will show that, with this minimum set of parameters, we can get a reasonable account of α and deuteron elastic scattering and total reaction cross sections within rather large energy ranges. It is well known that effects of couplings between the elastic-scattering channel and the other reaction channels (e.g., inelastic scattering and breakup and transfer reactions) on optical model potentials cannot be simply represented by renormalization of the potentials [28–31]. The study of these effects is out of the scope of this paper. Here, we are interested in the bulk properties of interactions between light composite particles with heavy targets. Thus, the experimental data are not meant to be best described with the present method, for which, hybrid methods with both phenomenological imaginary potentials and renormalized folding-model real potentials are often used in studies of elastic scattering of composite particles [2,3,9,13]. The questions in this paper are (i) to what extent can this minimum set of parameters reproduce experimental data within sufficiently large ranges of incident energy and target mass, and (ii) how do these parameters depend on incident energies?

This paper is organized as follows: A description of the SF model is given in Sec. II, and procedures of optical model analysis of the experimental data is described in Sec. III, where systematic optical model potential parameters for deuteron and α particles are obtained and are checked with angular distributions of elastic scattering and total reaction cross sections with optical model calculations. Comparisons with phenomenological systematic potentials are also made in this section. Discussions on corresponding nucleon-nucleus scattering, volume integral per interaction pair of the systematic OMPs, and transparency of nuclei to protons, deuterons, and α particles are made in Sec. IV. A summary and conclusions of this paper are made in Sec. V.

II. THE SF MODEL POTENTIAL

When applied to α-nucleus systems, the SF potential in Eq. (1) can be specified as

$$U^{\alpha}_{\rm SF}(R, E) = \sum_{i=p,n} \int \rho^{\alpha}_i(r) U_{i2}(|\boldsymbol{s}|, E_i)\, d\boldsymbol{r}, \qquad (2)$$

where E is the incident energy in the laboratory system. $\boldsymbol{s} = \boldsymbol{R} + \boldsymbol{r}$ is the vector from the c.m. of the target to position $\boldsymbol{r}$. The proton and neutron densities in ^{4}He at a position $\boldsymbol{r}$, $\rho^{\alpha}_i(r)$ $(i = p, n)$, are assumed to be equal and are taken to have Gaussian shapes with parameter $b = 1.1932$ fm (version C in Table I of Ref. [9]). This form of density distribution is found to be most realistic for an α particle [2,9]. The corresponding root-mean-square (rms) radius of an α particle is 1.461 fm, which is very close to its experimental value 1.47 ± 0.02 fm [9]. For a deuteron-target system, the SF potential is as follows:

$$U^{d}_{\rm SF}(R, E) = \sum_{i=p,n} \int \phi^{*}_0(\boldsymbol{r}) [U_{i2}(|\boldsymbol{s}|, E_i)] \phi_0(\boldsymbol{r})\, d\boldsymbol{r}, \qquad (3)$$

where $\boldsymbol{s} = \boldsymbol{R} \pm \boldsymbol{r}/2$ with $\boldsymbol{r}$ being the vector between the proton and the neutron in the deuteron, the upper and lower signs are for neutron and proton, respectively, and $\phi_0(\boldsymbol{r})$ is the ground-state wave function of the deuteron, which is a solution of the Schrödinger equation with a Gaussian p-n potential $V_{np}(r) = -V_0 \exp(-r^2/r_0^2)$ with $V_0 = 72.15$ MeV and $r_0 = 1.484$ fm. This potential reproduces the experimental deuteron binding energy of 2.226 MeV. The rms radius of this wave function is 3.857 fm. For simplicity, only the S component in the ground state of the deuteron, which is normalized to 1, is used. In both Eqs. (2) and (3), incident energies for the corresponding proton and neutron scatterings from the target nucleus are assumed to be

$$E_{i=p,n} = E/A_P, \qquad (4)$$

where A_P is the mass of the α particle or deuteron in atomic mass units.

The nucleon-target potentials U_{i2} in Eqs. (2) and (3) are calculated with the Lane-consistent JLMB model [25], which was derived from the nucleon potential in nuclear matter (NM) with the improved local density approximation (iLDA) [24,27],

$$U_{i2}(s, E_i) = \frac{1}{(t\sqrt{\pi})^3} \int \frac{U_{\rm NM}[\rho(r'), \alpha(r'), E_i]}{\rho(r')} \times \exp(-|\boldsymbol{s} - \boldsymbol{r}'|^2/t^2) \rho(r')\, d\boldsymbol{r}', \qquad (5)$$

where $\rho(r') = \rho_p(r') + \rho_n(r')$ is the NM density at position $\boldsymbol{r}'$ from the c.m. of the target and $\alpha(r') = [\rho_n(r') - \rho_p(r')]/\rho(r')$. The range of Gaussian form factor t can take different values for real and imaginary potentials, denoted as t_r and t_i, respectively. These form factors do not change volume integrals of the nucleon-nucleus potentials and those of the corresponding nucleus-nucleus OMPs, but allow one to fine-tune the geometry of the potentials so as to better reproduce experimental data. The $U_{\rm NM}/\rho(r')$ term in Eq. (5) is often taken to be the equivalent nucleon-nucleon interaction between a nucleon in a projectile with a nucleon in a target nucleus at position $\boldsymbol{r}'$ with local NM density $\rho(r')$ [32,33]. With the form of Eq. (5) we explicitly mean that we are adopting the *target position* prescription of the iLDA, which is suggested to be the best prescription for heavy targets [24]. In the JLMB model, the NM potential for a given NM density $\rho = \rho_p + \rho_n$

and asymmetry $\alpha = (\rho_n - \rho_p)/(\rho_n + \rho_p)$ is as follows:

$$U_{\rm NM}(E_i)_{\rho,\alpha} = \lambda_V(E_i)[V_0(\tilde{E}_i) \pm \lambda_{V1}(E_i)\alpha V_1(\tilde{E}_i)] + i\lambda_W(E_i)[W_0(\tilde{E}_i) \pm \lambda_{W1}(E_i)\alpha W_1(\tilde{E}_i)], \quad (6)$$

in which the + and − signs are for neutron and proton potentials, respectively. The nucleon energies $\tilde{E}_i$, used in calculations of the isoscalar (V_0 and W_0) and isovector (V_1 and W_1) potentials, are $E_p^{\rm c.m.} - V_C(s)$ and $E_n^{\rm c.m.}$, respectively, and

$$E_i^{\rm c.m.} = \frac{E_i A_T}{A_T + 1} \qquad (i = p, n), \quad (7)$$

with A_T being the mass of the target nucleus in atomic units, are the c.m. energies of the nucleon-target systems. For Coulomb corrections to proton incident energies [26,27], the Coulomb potential encountered by a proton is evaluated by assuming a uniform charge distribution of the target nucleus with charge radius $R_C = r_C \times A_T^{1/3}$ where $r_C = 1.123A_T^{1/3} + 2.35A_T^{-1/3} - 2.07A_T^{-1}$ (in femtometers) [26]. Details of the calculations for the isoscalar and isovector potentials and their corresponding normalization factors λ_V, λ_W, λ_{V1}, and λ_{W1} can be found in Refs. [24,25]. The parameters D and E_0 in Eqs. (14) and (22) of Ref. [24] are taken to be 126.25 MeV^2 and 9 MeV, respectively, instead of 625 MeV^2 and 10 MeV, respectively, in their original paper [34]. These corrected values are used in the program MOM [35].

The SF potentials have to be renormalized to better reproduce experimental data. Thus, the optical model potentials responsible for elastic scattering of the α particle and the deuteron in the present paper are as follows:

$$U(R, E) = N_r {\rm Re}[U_{\rm SF}(R, E)] + iN_i {\rm Im}[U_{\rm SF}(R, E)] + V_C(R), \quad (8)$$

where N_r and N_i are the renormalization factors for the real and imaginary potentials, respectively. The Coulomb potential V_C is calculated by assuming a uniformly distributed charge sphere of radius $R_C = r_C(A_T^{1/3} + A_P^{1/3})$ for α-nucleus scattering and $R_C = r_C A_T^{1/3}$ for deuteron-nucleus scattering with $r_C = 1.3$ fm. So eventually, we have four free parameters, t_r, t_i, N_r, and N_i, in our model. It is the task of this paper to study the energy dependence of these parameters. Note that, since the main purpose of including deuteron elastic scattering into the present analysis is to compare the values of its OMP parameters and their energy dependence with those of the α particle, the spin-orbit potential for the deuteron is not taken into account in this paper.

Proton, neutron, and NM density distributions in target nuclei needed in the calculations of the JLMB model potentials were obtained from Hartree-Fock (HF) calculations based on the SkX parametrization [36]. This parameter set accounts for the differences of binding energies for mirror nuclei [37], interaction cross sections [38], and nuclear charge distributions [39]. Recently, density distributions with this parameter set have also been used in transfer reactions [40]. The rms radii for proton, nucleon, and charge distributions from these calculations are listed in Table I. For comparison, the same quantities from the HF-Bogoliubov (HFB) calculations with the finite-range density-dependent Gogny force used in Ref. [25] and their corresponding experimental values are also shown. One sees that all calculations reproduce the experimental results reasonably well.

TABLE I. Comparison between density distributions used in Ref. [25] [HFB and HF + random-phase-approximation (RPA) calculations] and in the present analysis (HF) and their experimental values [41].

	$\langle r_n^2\rangle^{1/2}$ (fm)	$\langle r_p^2\rangle^{1/2}$ (fm)	$\langle r_{ch}^2\rangle^{1/2}$ (fm)
^{58}Ni expt.	3.700	3.686	3.772
^{58}Ni HFB	3.702	3.688	3.758
^{58}Ni HF	3.675	3.683	3.776
^{90}Zr expt.	4.289	4.204	4.280
^{90}Zr HFB	4.267	4.219	4.270
^{90}Zr HF	4.264	4.191	4.260
^{116}Sn expt.	4.692	4.546	4.619
^{116}Sn HFB	4.656	4.562	4.610
^{116}Sn HF	4.629	4.543	4.621
^{208}Pb expt.	5.593	5.453	5.503
^{208}Pb HF + RPA	5.653	5.465	5.515
^{208}Pb HF	5.597	5.441	5.498

III. ANALYSIS OF ^{4}He AND DEUTERON ELASTIC SCATTERING

A. Experimental data

By following the suggestions of Bauge *et al.* that the iLDA adopted in the JLMB model may not be a sufficiently good prescription for light targets [24], we limit our study to heavy targets with $A \geqslant 40$. Also, since the JLMB model parameters were derived from data with proton energies larger than around 10 MeV, we set the lower limit of the energy range in our analysis to 10 MeV/nucleon. The upper limit of the energy range is set at 100 MeV/nucleon. Beyond which, neglect of the relativistic effect in our calculations is expected to be nontolerable. Based on the considerations above, the targets selected in this paper are ^{58}Ni, ^{90}Zr, and ^{208}Pb, for which experimental data exist that cover large ranges of incident energies. Additionally, α-particle elastic scattering from ^{116}Sn at 240, 288, 340 and 386 MeV is included as a complement to the ^{90}Zr data at this energy range. The experimental data and their references are listed in Table II. All of them were taken from the nuclear reaction database EXFOR/CSISRS [70] except for those of α elastic scattering from ^{208}Pb at 40, 60, and 80 MeV, which were digitalized from the original paper.

B. Procedures of data analysis

For each set of data, 25 sets of SF potentials were calculated with t_r and t_i values, which vary from 0.8 to 2.0 fm with steps of 0.05 fm. Throughout this paper, the t_i values were assumed to be the same as t_r because we found that constraints of elastic-scattering angular distributions on the former is relatively weaker than that on the latter. These parameters

TABLE II. Experimental data (incident energies in MeV) and their references included in the present paper.

System	E_{lab}	Ref.	E_{lab}	Ref.	E_{lab}	Ref.
^{4}He + ^{58}Ni	43	[42]	49	[43]	52.4	[44]
	58.9	[44]	82	[44]	85.6	[44]
	58	[45]	104	[46]	139	[47]
	172.5	[48]	240	[49]	288	[50]
	340	[50]	386	[51]		
^{4}He + ^{90}Zr	40	[52]	50.1	[52]	59.1	[10]
	79.5	[10]	99.5	[10]	104	[46]
	118	[11]	141.7	[12]	386	[51]
^{4}He + ^{116}Sn	240	[53]	288	[50]	340	[50]
	386	[51]				
^{4}He + ^{208}Pb	40	[54]	60	[54]	80	[54]
	58	[55]	104	[46]	139	[47]
	288	[50]	340	[50]	386	[51]
d + ^{58}Ni	22	[56]	52	[57]	56	[58]
	79	[59]	120	[60]	170	[61]
	200	[62]				
d + ^{90}Zr	22	[56]	23.2	[63]	28.8	[64]
	34.4	[65]	56	[58]	183	[66]
d + ^{208}Pb	52	[57]	56	[58]	58.7	[67]
	80	[68]	85	[67]	110	[60]
	140	[69]				

are designated as t_{ri} in the following text. The computer code JLM was adapted for calculations of the JLMB model nucleon-nucleus potentials [71]. Renormalization factors, N_r and N_i, of the potentials with each t_{ri} value were found by fitting experimental data with standard minimum χ^2 (divided by the number of data points) method. Experimental uncertainties were used if they were available, otherwise, uniform uncertainties of 10% were applied for all data points. Since different measurements have different systematic uncertainties, we also allow normalizations of experimental data N_o to vary in the fittings. The optical model fittings were performed by using computer code SFRESCO, which is a combination of FRESCO [72] and the search routine MINUIT [73]. To minimize the dependence on their initial values, nine pairs of initial values for N_r and N_i were used in the fittings. So for each projectile-target system at each incident energy, we obtain 225 ($= 25 \times 9$) sets of $\{t_{ri}, N_r, N_i, N_o, \chi^2\}$ numbers, among which, the smallest χ^2 value $\chi^2_{\min}$ was found. We then take the $\{t_{ri}, N_r, N_i, N_o\}$ values whose corresponding χ^2 values are not larger than $\eta \times \chi^2_{\min}$ as *reasonable* parameters. *Local* potential parameters, which account for the projectile scattering from one target nucleus at one incident energy, can then be obtained by averaging these reasonable parameters weighted with their corresponding $(1/\chi^2)^2$ values. Standard deviations of these local parameters were obtained simultaneously. Various η values within the range of $1.1 \leqslant \eta \leqslant 1.5$ were applied, and the local potential parameters were found to be nearly independent of it, thus, we chose $\eta = 1.2$ in our analysis. The resulting local potential parameters and their corresponding χ^2 values and volume integrals per interaction pair are listed in Tables III and IV for α particles and deuterons, respectively.

TABLE III. Local potential parameters and their corresponding values of χ^2 and volume integral per interaction pair for α particles, where E are in MeV, t_{ri} are in femtometers, and J_r and J_i are in MeV fm^3.

	E	t_{ri}	N_r	N_i	χ^2	J_r	J_i
α + ^{58}Ni	43.0	1.39	0.71	0.81	24.2	−305.3	−69.7
	49.0	1.29	0.72	0.77	16.9	−307.9	−70.2
	52.4	1.43	0.72	0.77	7.9	−305.9	−71.9
	58.9	1.48	0.76	0.77	9.2	−320.9	−73.7
	58.0	1.41	0.77	0.87	10.4	−322.7	−82.7
	67.7	1.45	0.77	0.86	7.6	−318.9	−81.7
	82.0	1.50	0.74	0.92	6.5	−297.9	−86.1
	85.6	1.37	0.75	0.97	4.3	−299.4	−91.1
	104.0	1.43	0.73	1.05	18.5	−283.2	−101.2
	139.0	1.70	0.79	1.00	5.2	−287.3	−100.4
	172.0	1.60	0.77	0.95	4.7	−261.6	−97.1
	240.0	1.50	0.76	1.23	3.2	−225.2	−127.4
	288.0	1.80	0.79	0.89	14.3	−213.8	−93.3
	340.0	1.84	0.90	1.16	19.1	−217.4	−123.1
	386.0	1.75	0.88	1.12	20.1	−191.2	−122.8
α + ^{90}Zr	40.0	1.31	0.77	0.74	35.4	−332.0	−56.5
	59.1	1.42	0.76	0.79	18.9	−317.7	−70.3
	79.5	1.36	0.75	0.96	19.3	−301.4	−83.9
	99.5	1.40	0.75	1.01	19.8	−292.8	−90.3
	104.0	1.45	0.74	1.02	2.2	−283.7	−92.5
	118.0	1.45	0.75	1.00	10.1	−281.8	−92.7
	141.7	1.57	0.78	0.98	3.8	−278.6	−94.2
	386.0	1.83	0.89	1.08	15.8	−195.7	−117.3
α + ^{116}Sn	240.0	1.65	0.80	1.12	4.1	−239.7	−111.1
	288.0	1.96	0.79	0.90	11.8	−214.9	−90.4
	340.0	1.96	0.88	1.06	20.7	−214.7	−109.8
	386.0	1.87	0.87	1.07	23.2	−191.1	−114.9
α + ^{208}Pb	40.0	1.52	0.81	0.92	0.1	−345.3	−56.8
	58.0	1.35	0.77	0.87	25.9	−317.1	−64.2
	60.0	1.50	0.81	0.94	0.6	−333.3	−69.7
	80.0	1.50	0.74	0.97	1.1	−296.9	−73.9
	104.0	1.55	0.77	1.19	8.5	−296.7	−93.2
	139.0	1.49	0.84	1.22	14.0	−304.2	−102.8
	288.0	1.93	0.78	0.89	21.7	−213.0	−85.3
	340.0	1.95	0.87	1.03	21.5	−214.1	−103.0
	386.0	1.93	0.91	1.16	40.9	−202.9	−120.9

It is well known that OMPs from the analysis of elastic-scattering data at low energies suffer from continuum and discrete ambiguities (see, e.g., Chap. 12 of Ref. [1]). No apparent continuum ambiguities were found in this paper by examining the correlations of potential parameters, for instance, between t_{ri} and N_r. However, distinguished discrete ambiguities in N_r do show up for low-energy scattering data. For these cases, the *physical* families of N_r had to be selected before the *reasonable* parameters were collected, by tracing their families to a higher-energy region, where the discrete ambiguities disappeared.

TABLE IV. Local potential parameters and their corresponding values of χ^2 and volume integral per interaction pair for deuterons, where E are in MeV, t_{ri} are in femtometers, and J_r and J_i are in MeV fm^3. The exceptionally large χ^2 for ^{208}Pb at 140 MeV is caused by the very small experimental error bar obtained from the nuclear database.

	E	t_{ri}	N_r	N_i	χ^2	J_r	J_i
$d + {}^{58}$Ni	20.0	0.92	0.88	1.25	13.5	−381.2	−103.2
	22.0	0.91	0.92	1.20	17.4	−391.9	−103.4
	52.0	1.24	0.95	1.15	10.7	−365.9	−110.2
	56.0	1.13	0.96	1.20	7.5	−362.7	−116.6
	79.0	1.40	1.09	1.21	7.1	−377.9	−122.6
	120.0	1.35	1.04	1.20	2.4	−307.4	−124.0
	170.0	1.30	1.14	1.30	29.7	−275.3	−136.3
	200.0	1.13	1.19	1.41	6.1	−252.2	−154.7
$d + {}^{90}$Zr	22.0	1.06	0.87	1.16	17.7	−371.3	−91.8
	23.2	1.03	0.90	1.19	10.4	−381.9	−96.5
	28.8	0.97	0.93	1.03	14.8	−385.3	−90.6
	34.4	0.97	0.96	1.14	12.7	−390.7	−100.1
	56.0	1.27	0.95	1.18	8.7	−359.1	−107.7
	183.0	1.30	1.19	1.28	4.0	−271.4	−135.5
$d + {}^{208}$Pb	52.0	1.38	0.87	1.31	19.4	−333.3	−102.6
	56.0	1.21	0.85	1.26	15.1	−321.5	−99.2
	58.7	1.17	0.88	1.27	18.7	−327.3	−101.7
	80.0	1.50	0.95	1.26	14.9	−331.0	−108.3
	85.0	1.15	0.96	1.18	10.8	−325.2	−103.5
	110.0	1.43	1.02	1.26	5.1	−316.4	−115.9
	140.0	1.33	1.06	1.33	1430.8	−293.3	−126.8

C. Energy dependence of potential parameters

In this section, we fit the local potential parameters with some functions of incident energy to get the *global* potential parameters for α particles and deuterons. Note that functions reported in the following subsections were chosen primarily to reflect the energy variations of these potential parameters. There are no specific physical considerations behind them except that we always avoid choosing functions that may extend the parameters for values that are very wrong, such as negative values, to physical intuitions.

1. Energy dependence of t_{ri}

The most significant effect of t_{ri} is in the form factors of the resulting SF potentials. As an example, in Fig. 1, we show how the SF potential, which corresponds to α elastic scattering ^{90}Zr at 141.7 MeV, depends on values of t_{ri}. One can see that the diffuseness of the potential increases, and correspondingly, its rms radius decreases, with an increase in t_{ri}. The same is found for the imaginary potential.

The local and global values of t_{ri} for α- and deuteron-nucleus potentials are shown in Fig. 2 as functions of $E_{\text{c.m.}}/A_P$. The values of t_{ri} seem to saturate at 1.9 fm for α particles and saturate or reach their maximum values at around 1.35 fm for deuterons. Note that, in Ref. [27], these finite-range parameters were estimated to be smaller than 2.4 fm, which is reasonably well satisfied by the present results. We represent the global

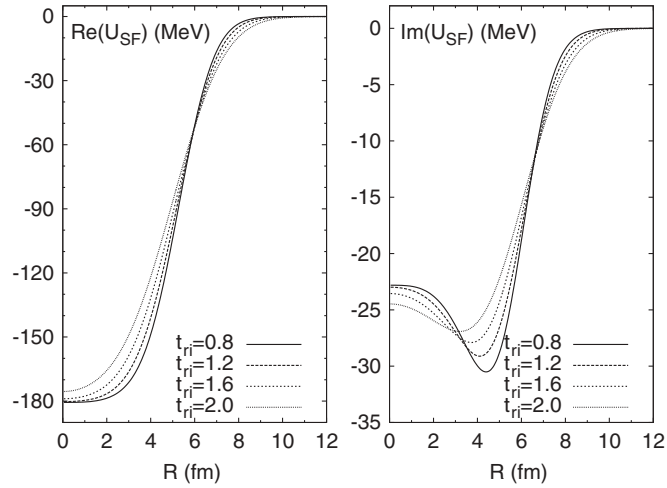

FIG. 1. SF potential for ^{4}He elastic scattering from ^{90}Zr at 141.7 MeV calculated with different values of the range parameter t_{ri}.

values of t_{ri} for an α particle by

$$t_{ri}^{\alpha}(e_{\text{c.m.}}) = 1.93 - \frac{0.552}{1 + \exp[(e_{\text{c.m.}} - 48.6)/15.2]}, \quad (9)$$

and for a deuteron by

$$t_{ri}^{d}(e_{\text{c.m.}}) = 0.592 + 2.21e^{-0.0114e_{\text{c.m.}}}(1 - e^{-0.0185e_{\text{c.m.}}}), \quad (10)$$

where

$$e_{\text{c.m.}} = \frac{E_{\text{c.m.}}}{A_P} = \frac{A_T}{A_P(A_P + A_T)}E_{\text{lab}}. \quad (11)$$

The increase in t_{ri} values, which corresponds to an increase in the potential diffuseness and a decrease in the potential radius for the same projectile-target system, with the increase in incident energies shown in Fig. 2 for α potentials agrees with the results of many other investigations, for example, those in Refs. [44,50]. This result clearly suggests that energy dependence of the geometry parameters has to be taken into

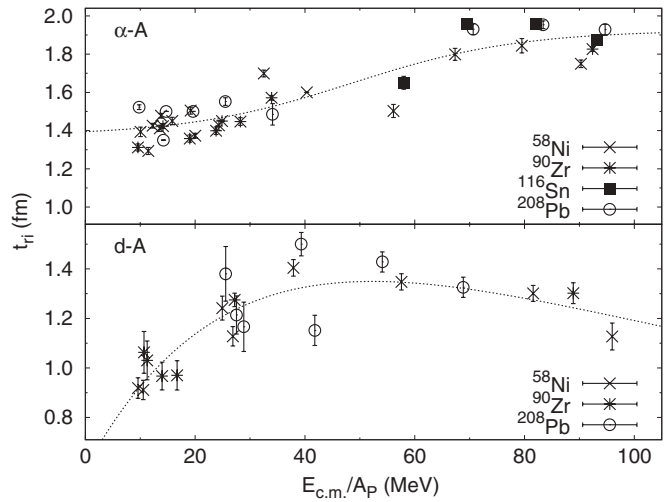

FIG. 2. Energy dependence of t_{ri} for ^{4}He and deuteron with heavy targets.

account properly if a systematic study of α-nucleus scattering within a wide energy range is to be made. This makes the α particle different from a proton and a neutron, for which global optical potentials could be obtained within rather large energy ranges with fixed t_r and t_i values [24,25]. Our result for the deuteron qualitatively agree with the phenomenological global deuteron potential by Daehnick *et al.*, whose real potential diffuseness parameter increases linearly with the increase in incident energy [74]. Energy dependence of geometry parameters might be common for composite projectiles. To revisit the existing phenomenological global potentials for deuterons [75] and for ^{3}He and ^{3}H [7,76,77] with respect to this point would be interesting.

2. Energy dependence of N_r and N_i

The local values of N_r and N_i are shown as symbols in Fig. 3 for α particles and deuterons. Their global values, as functions of $E_{\rm c.m.}/A_P$, represented by Eqs. (12)–(15), are shown as dashed curves in the same figure,

$$N_r^{\alpha}(e_{\rm c.m.}) = 0.887 - \frac{0.123}{1+e^{(e_{\rm c.m.}-73.0)/2.23}}, \quad (12)$$

$$N_i^{\alpha}(e_{\rm c.m.}) = 0.615 + 1.34e^{-0.0101e_{\rm c.m.}}(1-e^{-0.0178e_{\rm c.m.}}), \quad (13)$$

$$N_r^{d}(e_{\rm c.m.}) = 1.45 - 0.557e^{-e_{\rm c.m.}^2/11750}, \quad (14)$$

$$N_i^{d}(e_{\rm c.m.}) = 1.64 - \frac{0.690}{1+e^{(e_{\rm c.m.}-73.0)/80.8}}. \quad (15)$$

N_r values of the α particle change from around 0.75 to around 0.89 from lower to higher energies. This corresponds to reductions in the SF potentials from 25% to 11%. By taking effects of energy dependence of constituent nucleons and three-body terms into account, Perkin *et al.* [4] estimated the reduction to be 14.2% for the α potential. This is very close to the reduction factor of 15% obtained by Jackson and Johnson [8], which was found to be a consequence of nonlocality of the nucleon-nucleus potential and finite size

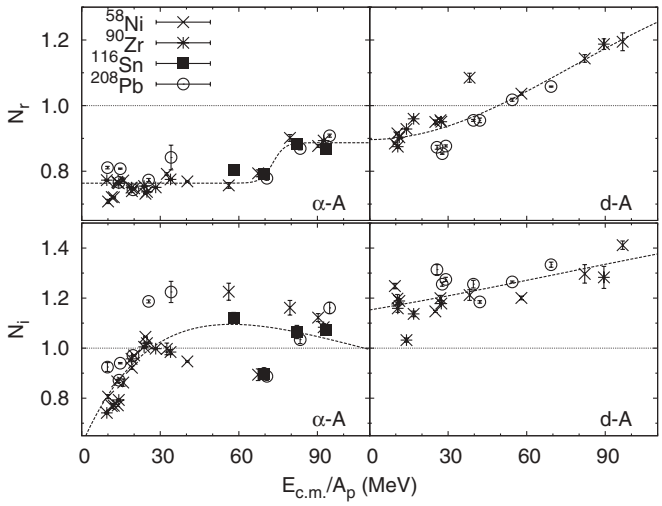

FIG. 3. Energy dependence of N_r and N_i for an α particle and a deuteron with heavy targets.

of the projectile. However, both theories underestimate the α-potential reduction factors at lower energies. As discussed in Ref. [4], Pauli principle also contributes to these reduction factors, and its effect increases as incident energy decreases. The quoted reduction factors from both theories, however, do not include effects of Pauli principle. By keeping this fact in mind, the N_r values for the α particles obtained in this paper seem to qualitatively agree with both theoretical estimations. Note that renormalization factors of an α particle in the double-folding model analysis with realistic nucleon-nucleon interactions, such as CDM3Y6 [78] were found to be around 1.1–1.2 [3,9,78]. They should not be contradicted by the N_r values obtained in this paper because of the difference in nucleon potentials used.

Theoretical understanding of the absolute values of N_i and their energy dependence may be more challenging. The JLMB model nucleon-nucleus potential is known to account well for the *free* nucleon-nucleus scattering and reactions [24,25]; they effectively include effects of couplings to other channels, such as excitations of the target nucleus. These couplings are likely to be quite different when the nucleon is bound in another nucleus [2]. Because of this consideration, the energy dependence of N_i for the α particle and its value close to unity within 20% seems to be rather surprising. Note that the averaged value of N_i being close to unity was also found for $1p$-shell nuclei by Trache *et al.* [33].

Systematic differences in N_r and N_i values are clearly seen between α and deuteron potentials. Reductions of the real SF potentials for deuteron-nucleus scattering are observed at low-energy regions. These reduction factors also quantitatively agree with the theoretical predictions of Refs. [4,8]. However, the N_r values for the deuteron are larger than unity when $E_{\rm c.m.}/A_P$ is larger than around 40 MeV, which is not predicted by both theories. The N_i values for deuterons are systematically larger than those for α particles, and they increase with an increase in incident energies. Because of the weak-binding nature of the deuteron, one would expect that these phenomena may, at least partially, relate to the energy dependence of the effects of couplings to continuum states of the deuteron in the scattering processes. However, quantitative theoretical explanations are needed. It is also worth noting that many studies have shown that coupling effects to optical potentials cannot simply be represented by uniform renormalization of the potentials over the entire radial ranges [28,31]. It would be interesting to see whether there are some relations between N_r and N_i values and the binding energies of incident particles. This would be useful for applications of the SF model with the JLMB model potential for other composite projectiles. For this purpose, it would be interesting to analyze the ^{3}He and ^{3}H elastic scattering in the same manner.

D. Applications of the global potentials

1. Angular distributions of differential cross sections

Comparisons between experimental angular distributions of differential cross sections for α- and deuteron-nucleus elastic scattering and theoertical calculations with both local (solid curves) and global potential parameters (dashed curves) are

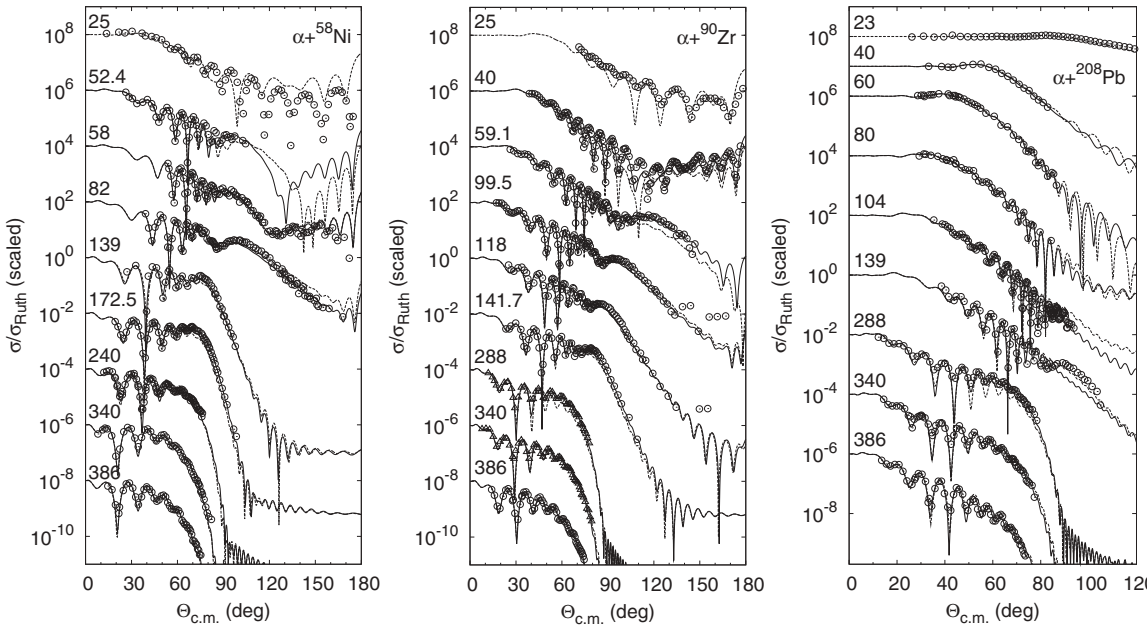

FIG. 4. Comparison between optical model calculations and experimental data of ^{4}He elastic scattering from ^{58}Ni, ^{90}Zr (triangles for the ^{116}Sn target at 288 and 340 MeV), and ^{208}Pb at different energies. The solid and dashed curves were calculated with local and global potential parameters, respectively. Different data sets are offset by factors of 10^{n} with an n variable for optimum view. The ^{58}Ni data at 25 MeV, ^{90}Zr data at 25 MeV, and ^{208}Pb data at 23 MeV are from Refs. [79–81]. Experimental error bars are not shown in these figures.

shown in Figs. 4 and 5. In general, experimental data can be satisfactorily described, including data at intermediate energies that show the well-known nuclear rainbow phenomena (see Fig. 6 for a clearer view). The global potential parameters give results as close as the local ones. Comparisons with experimental data that were not included in the global analysis at low-energy ranges were also performed. To see the angular distributions at higher energies more clearly, which are usually measured at very limited angular ranges, we translate the c.m. angles $\theta_{\mathrm{c.m.}}$ into

$$\Theta_{\mathrm{c.m.}} = (1 + E^{1/4} \times e^{-\theta_{\mathrm{c.m.}}/w}) \times \theta_{\mathrm{c.m.}}, \tag{16}$$

in Figs. 4 and 5, where w is taken to be 30°. The units of $\theta_{\mathrm{c.m.}}$ and $\Theta_{\mathrm{c.m.}}$ are degrees. Although this translation of angles will make it difficult to read some information, for instance, the rainbow angle at a certain energy directly from the figures,

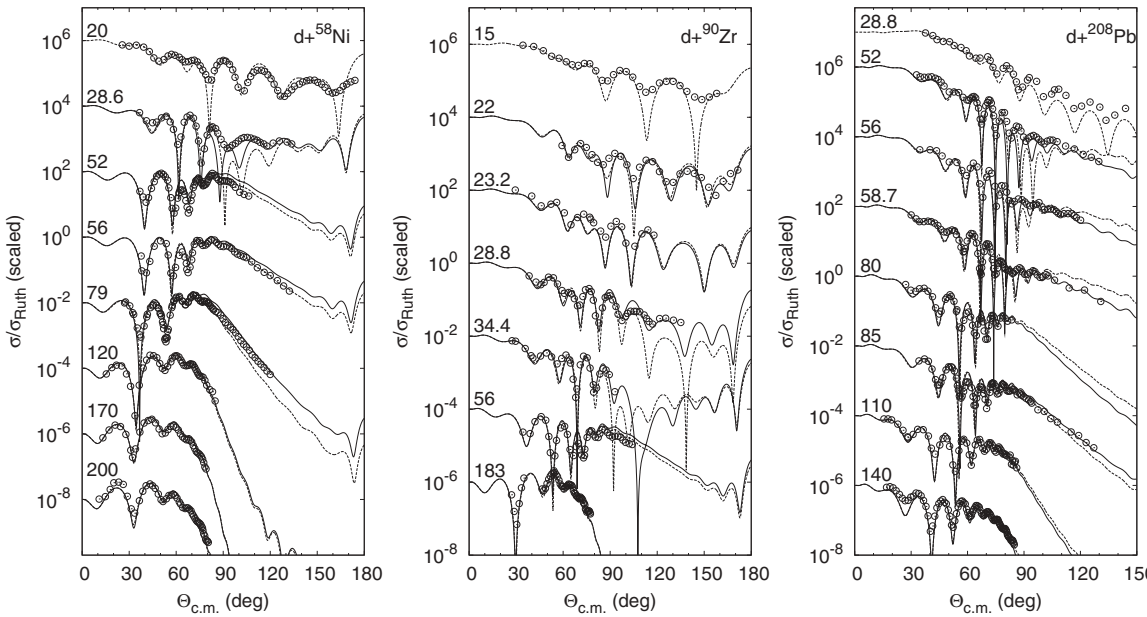

FIG. 5. Same as Fig. 4 but with deuteron projectiles. The ^{58}Ni data at 20 MeV, ^{90}Zr data at 15 MeV, and ^{208}Pb data at 28.8 MeV are from Refs. [63,64,82].

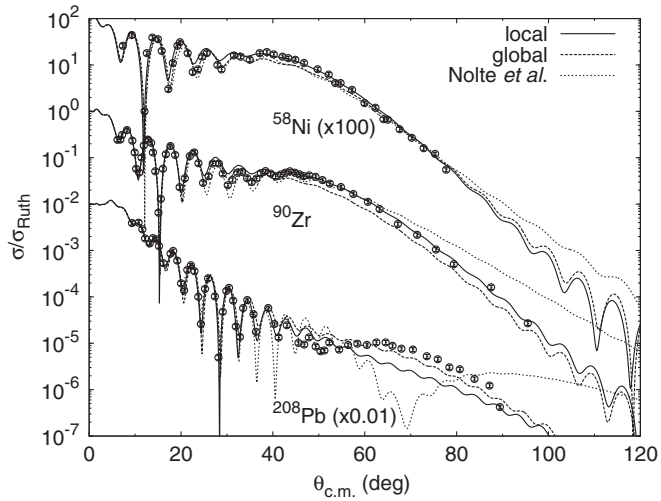

FIG. 6. Comparison between optical model calculations and experimental data for α elastic scattering at around 140 MeV as an example of a detailed view for the degree of agreement with model calculations and data. Note that the c.m. angles are $\theta_{\text{c.m.}}$ in this figure.

we take it as the best way to present several data, which cover large enough energy ranges, in the same figure. Figure 7 shows the effect of these transformations: The maximum scattering angles are transformed from around 30° in this figure to around 90° in Fig. 4.

2. *Total reaction cross sections*

Total reaction cross sections (σ_R) are also useful to constrain the OMP parameters. These data were not included in the present paper. Instead, we use these data to check the validity of the global potentials. We compare the optical model predictions of total reaction cross sections for the α and deuteron interactions with ^{58}Ni, ^{116}Sn, and ^{208}Pb and their experimental values. The results are shown in Figs. 8 and 9 for

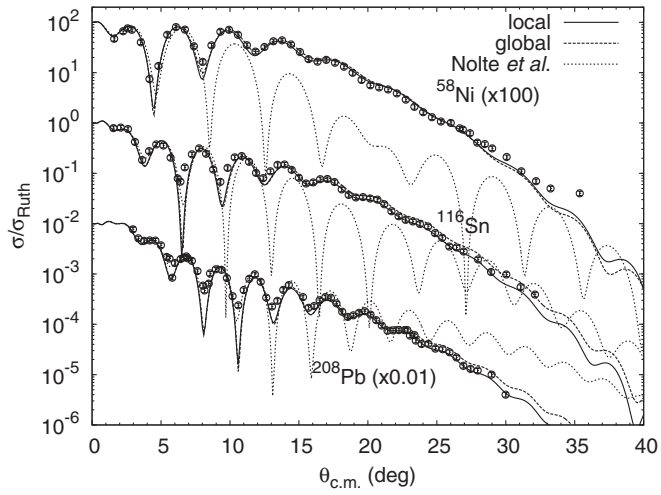

FIG. 7. Comparison between optical model calculations and experimental data for α elastic scattering at 340 MeV. Note that the c.m. angles are $\theta_{\text{c.m.}}$ in this figure.

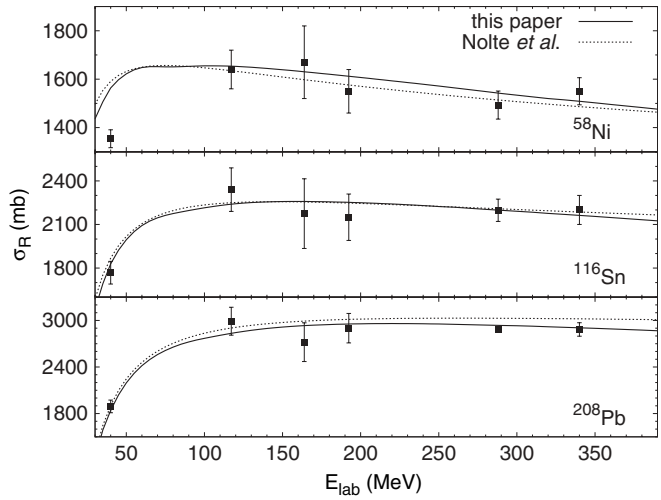

FIG. 8. Comparison between optical model calculations of total reaction cross sections and experimental data for the α particle. The target nuclei are indicated in the figure. The experimental data are from Refs. [83,84].

α particles and deuterons, respectively. Very good agreement between theoretical calculations and experimental data were found for α-nucleus systems. Theoretical values of σ_R agree rather well with the experimental data for the d-^{58}Ni system, however, they underestimate those for the d-^{116}Sn system by around 5% and for the d-^{208}Pb system by around 10%. Note that similar phenomena (i.e., the increase in underestimation of σ_R by theoretical calculations with the increase in the target masses) has also been observed in proton-nucleus systems [24]. The reasons for these underestimations and their increase in target mass numbers shown for proton- and deuteron-nucleus systems and not for α-nucleus systems are not clear at the moment. Note that, for the ^{116}Sn target, only α

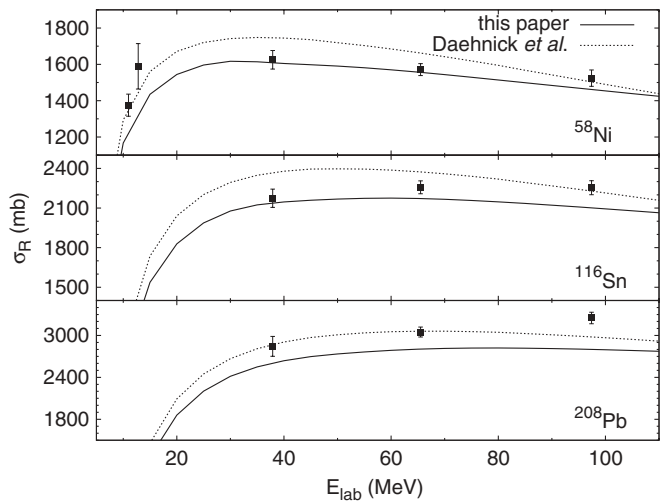

FIG. 9. Comparison between optical model calculations of total reaction cross sections and experimental data for the deuteron. The target nuclei are indicated in the figure. The experimental data are from Refs. [85–87].

scattering data at energies larger than 240 MeV were included in the derivation of the global potential parameters. Good agreements between theoretical and experimental σ_R values of the α-^{116}Sn system at low energies and of the d-^{116}Sn system indicate that the global potential derived in this paper is reliable in the heavy target region.

3. *Comparisons with phenomenological potentials*

Comparisons between the global parameters in Eqs. (9), (12), and (13) and the phenomenological global α potential of Nolte *et al.* (the Nolte potential) [20] are made in Figs. 6 and 7 for angular distributions and in Fig. 8 for total reaction cross sections. Similar comparisons were not shown in Figs. 4 and 5 to keep these figures clean. Comparisons with volume integrals per interaction pairs of the global potentials with those of Atzrott *et al.* [13] are made in Sec. IV B. Since the Nolte potential was derived only for a target mass up to 90, it is understandable that it is not suitable for heavier targets, such as ^{208}Pb. Also, since the Nolte potential was derived within a rather limited energy range around 140 MeV, geometry parameters of Woods-Saxon potentials were assumed to be independent of incident energy. As we discussed in Sec. III C, to ignore energy dependence of these parameters will make the Nolte potential fail to reproduce experimental data at higher energies, as clearly seen in Fig. 7. The total reaction cross sections from optical model calculations with the Nolte potential and the global potential reported in this paper, however, are rather close, and both potentials reproduce experimental data well. This may suggest that total reaction cross-sectional data are not sensitive to form factors of optical model potentials.

Similar comparisons between systematics in Eqs. (10), (14), and (15) and those of Daehnick *et al.* for the deuteron (the Daehnick potential) [74] are made in Figs. 9 and 10 for angular distributions and total reaction cross sections, respectively. These two potentials give similar angular distributions. But total reaction cross sections with the Daehnick potential are systematically larger than those with the potentials obtained in this paper. Both systematics, in general, cannot give satisfactory reproductions for total reaction cross-sectional data. The discrepancies may be caused by the fact that couplings to breakup channels, which are important for deuteron-induced reactions, are out of the scope of the optical model adopted in both studies.

IV. DISCUSSIONS

A. Nucleon-nucleus elastic scattering

As discussed in Sec. III C, t_{ri} for the α-nucleon systems increases as the incident energy increases. At high energies, this value reaches around 1.9 fm. On the other hand, the finite-range parameters used in the JLMB model for the global description of nucleon-nucleus elastic-scattering data are $t_r = 1.25$ and $t_i = 1.35$ fm. It is necessary to check whether the resulting nucleon-nucleus OMPs with t_{ri} values in this paper can still reasonably reproduce the experimental nucleon-nucleus scattering at higher energies. This is important because, otherwise, the SF model will lose its initial meaning. We examine this problem by using, as an example, proton elastic scattering from ^{90}Zr at 65 MeV, which corresponds to α energy of 260 MeV and the global t_{ri} value of 1.77 fm. Comparisons with angular distributions of experimental data and the optical model calculation with parameter set (1) $t_r = 1.25$ fm and $t_i = 1.35$ fm and (2) $t_r = t_i = 1.77$ fm are shown in Fig. 11. One can see that the amplitudes of differential cross sections at larger angles with parameter set (2) are smaller than those with set (1); however, the phases of experimental angular distributions, especially at smaller angles, seem to be better reproduced by set (2). The total reaction cross section with parameter set (1) is 1208.35 mb, while that with set (2) is 1261.94 mb. They differ by only 4%, which is smaller than typical experimental uncertainties. Thus, we justified that, even with relatively large t_r and t_i values, the JLMB model can still

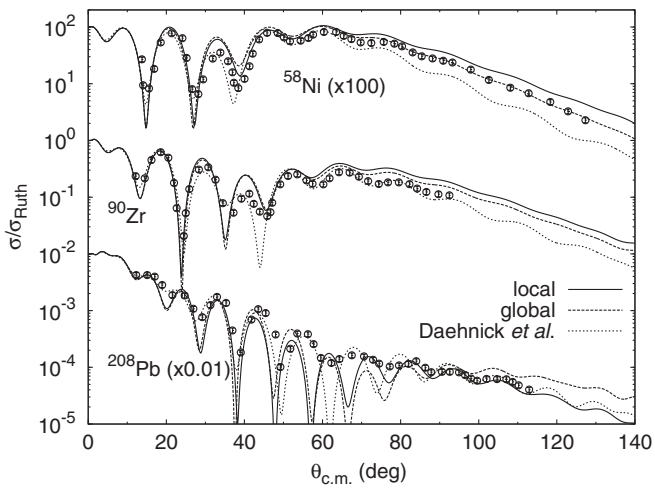

FIG. 10. Comparison between optical model calculations and experimental data for deuteron elastic scattering at 56 MeV. Note that the c.m. angles are $\theta_{\text{c.m.}}$ in this figure.

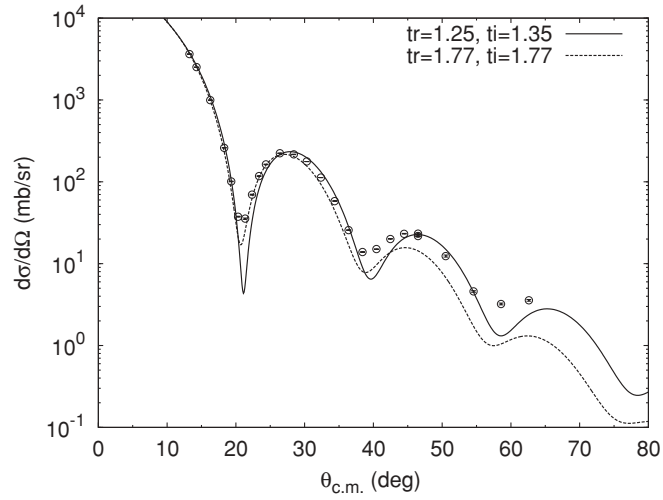

FIG. 11. JLMB model description of proton elastic scattering from ^{90}Zr with different finite-range Gaussian parameters. The experimental data are from Ref. [88].

give a reasonable account of the nucleon-nucleus scattering data.

B. Volume integrals of the global potentials

Volume integrals per interaction pair of the real and imaginary parts J_r and J_i, respectively, of the global α and deuteron potentials derived in this paper are shown in Fig. 12 for ^{58}Ni, ^{90}Zr, and ^{208}Pb. These quantities are defined as [2]

$$J_r(E) = \frac{1}{A_P A_T} \int N_r \mathrm{Re}[U_{\mathrm{SF}}(R, E)]\, d\boldsymbol{R}, \qquad (17)$$

and

$$J_i(E) = \frac{1}{A_P A_T} \int N_i \mathrm{Im}[U_{\mathrm{SF}}(R, E)]\, d\boldsymbol{R}. \qquad (18)$$

The same quantities for the proton and neutron at the same c.m. energy per nucleon are also shown. J_r values for the α potential agree very well with those obtained by Atzrott *et al.* [13], the averaged difference between common studied systems in both works is smaller than 3%. The averaged differences in J_i values, however, are 4%, 13%, and 20% for ^{58}Ni, ^{90}Zr, and ^{208}Pb, respectively. Since phenomenological imaginary potentials were used in Ref. [13] to get excellent reproductions of the α elastic-scattering data, these deviations may suggest some defeat in the present approach. Possible improvement of the present approach may be found if the constraint that t_i is equal to t_r is released.

C. Transparency of nuclei

It is known (e.g., by analyzing reaction cross-sectional data at intermediate energies with ^{12}C, ^{16}O, and ^{40}Ca nuclei [89, 90]) that nuclei are more transparent to protons and deuterons than to α particles. In terms of S-matrix elements S_L, where

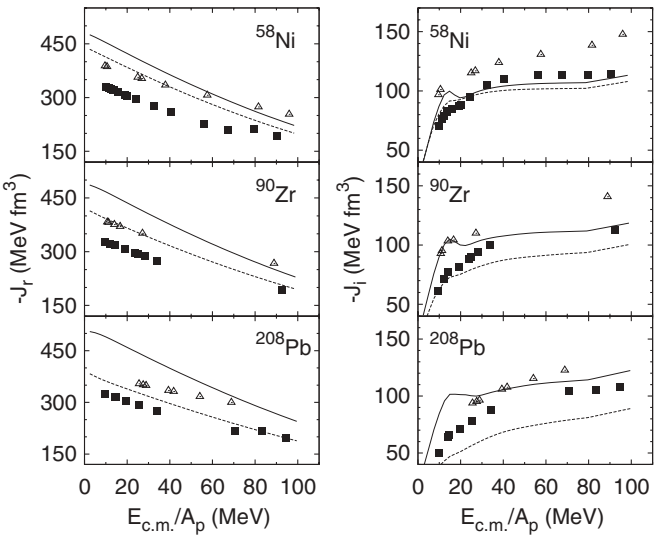

FIG. 12. Volume integrals per interaction pair of optical model potentials for a proton (solid curves), a neutron (dashed curves) with the JLMB model, and a deuteron (open triangles) and α (solid squares) with global SF model parameters.

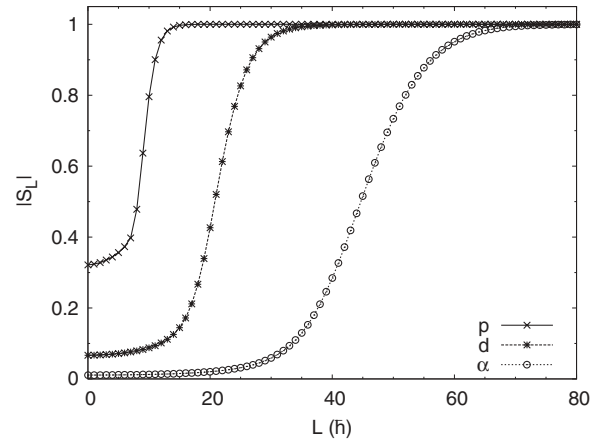

FIG. 13. Moduli of the S matrix for proton, deuteron, and α-particle elastic scattering from ^{58}Ni at 80 MeV/nucleon calculated with the JLMB model and the global parameters obtained in this paper.

L is the angular momentum related to the projectile-target relative motion, this phenomenon suggests that, with the same target masses and incident energies per nucleon, the S_L of α particles should be smaller than that of protons and deuterons at small L values. As an example, in Fig. 13, we plot the moduli of S_L from optical model calculations for the elastic scattering of proton, deuteron, and α particles from ^{58}Ni at 80 MeV/nucleon. The proton potential was obtained by using the JLMB model systematics, and the deuteron and α potentials were calculated with global potential parameters reported in this paper. One sees that our results agree with the known facts mentioned at the beginning of this subsection.

V. SUMMARY AND CONCLUSIONS

SF models with the JLMB nucleon-nucleus potentials were applied in the analysis of α and deuteron elastic scattering from heavy ions. Energy dependence of a minimum set of potential parameters t_{ri}, N_r, and N_i were derived, and global optical model potentials were obtained for both projectiles. Optical model calculations with the global potential parameters agree well with both angular distributions of elastic scattering and total reaction cross sections for α particles. The results of this paper suggest that a global optical model potential up to 100 MeV/nucleon for an α particle is possible if the energy dependence of potential form factors is taken into account appropriately.

Corrections to the SF model potentials caused by compositeness of projectiles were studied through renormalization factors N_r and N_i. The N_r values for the α particle qualitatively agree with theoretical estimations, while agreements in the N_r of the deuterons are seen only at low energies. Systematic differences were found between α and deuteron projectiles in their N_r and N_i values and their energy dependence, which may be related to the very different binding energies and structures of these two projectiles. Theoretical studies of the effects of the compositeness of projectiles on SF potentials

and their relations with renormalization factors studied in this paper are appealing.

ACKNOWLEDGMENTS

We thank the referee for helpful comments and suggestions. D. Y. Pang thanks Professor E. Bauge for help with the JLMB model calculations and Professor R. C. Johnson for helpful discussions. This work was supported by the National Basic Research Program of China (Grant No. 2007CB815002), the National Natural Science Foundation of China (Grants No. 11035001, No. 10775003, No. 10735010, and No. 10975006) and the China Postdoctoral Science Foundation (Grant No. 20100470133).

[1] G. R. Satchler, *Direct Nuclear Reactions* (Clearndon Press, Oxford, 1983).
[2] G. R. Satchler and W. G. Love, Phys. Rep. **55**, 183 (1979).
[3] M. E. Brandan and G. R. Satchler, Phys. Rep. **285**, 143 (1997).
[4] D. G. Perkin, A. M. Kobos, and J. R. Rook, Nucl. Phys. A **245**, 343 (1975).
[5] F. G. Perey and G. R. Satchler, Nucl. Phys. A **97**, 515 (1967).
[6] R. C. Johnson and P. J. R. Soper, Nucl. Phys. A **182**, 619 (1972).
[7] D. Y. Pang, P. Roussel-Chomaz, H. Savajols, R. L. Varner, and R. Wolski, Phys. Rev. C **79**, 024615 (2009).
[8] D. F. Jackson and R. C. Johnson, Phys. Lett. B **49**, 249 (1974).
[9] D. T. Khoa, Phys. Rev. C **63**, 034007 (2001).
[10] L. W. Put and A. M. J. Paans, Phys. Lett. B **49**, 266 (1974).
[11] L. W. Put and A. M. J. Paans, Nucl. Phys. A **291**, 93 (1977).
[12] D. A. Goldberg, S. M. Smith, and G. F. Burdzik, Phys. Rev. C **10**, 1362 (1974).
[13] U. Atzrott, P. Mohr, H. Abele, C. Hillenmayer, and G. Staudt, Phys. Rev. C **53**, 1336 (1996).
[14] A. A. Cowley and N. S. Wall, Phys. Rev. C **17**, 1322 (1978).
[15] F. Michel, G. Reidemeister, and S. Ohkubo, Phys. Rev. C **61**, 041601(R) (2000).
[16] P. P. Singh, P. Schwandt, and G. C. Yang, Phys. Lett. B **59**, 113 (1975).
[17] A. M. Kobos, B. A. Brown, R. Lindsay, and G. R. Satchler, Nucl. Phys. A **425**, 205 (1984).
[18] P. Demetriou, C. Grama, and S. Goriely, Nucl. Phys. A **707**, 253 (2002).
[19] M. Avrigeanu, A. C. Obreja, F. L. Roman, V. Avrigeanu, and W. von Oertzen, At. Data Nucl. Data Tables **95**, 501 (2009).
[20] M. Nolte, H. Machner, and J. Bojowald, Phys. Rev. C **36**, 1312 (1987).
[21] X. H. Li, H. X. An, and C. H. Cai, Eur. Phys. J. A **39**, 255 (2009).
[22] R. L. Varner, W. J. Thompson, T. L. McAbee, E. J. Ludwig, and T. B. Clegg, Phys. Rep. **201**, 57 (1991).
[23] A. J. Koning and J. P. Delaroche, Nucl. Phys. A **713**, 231 (2003).
[24] E. Bauge, J. P. Delaroche, and M. Girod, Phys. Rev. C **58**, 1118 (1998).
[25] E. Bauge, J. P. Delaroche, and M. Girod, Phys. Rev. C **63**, 024607 (2001).
[26] J. P. Jeukenne, A. Lejeune, and C. Mahaux, Phys. Rev. C **15**, 10 (1977).
[27] J. P. Jeukenne, A. Lejeune, and C. Mahaux, Phys. Rev. C **16**, 80 (1977).
[28] N. Keeley and R. S. Mackintosh, Phys. Rev. C **77**, 054603 (2008).
[29] R. S. Mackintosh and N. Keeley, Phys. Rev. C **79**, 014611 (2009).
[30] V. Lapoux *et al.*, Phys. Rev. C **66**, 034608 (2002).
[31] A. A. Ioannides and R. S. Mackintosh, Phys. Lett. B **169**, 113 (1986).
[32] F. Carstoiu and M. Lassaut, Nucl. Phys. A **597**, 269 (1996).
[33] L. Trache, A. Azhari, H. L. Clark, C. A. Gagliardi, Y. W. Lui, A. M. Mukhamedzhanov, R. E. Tribble, and F. Carstoiu, Phys. Rev. C **61**, 024612 (2000).
[34] E. Bauge (private communication).
[35] T. Belgya *et al.*, IAEA Technical Report No. IAEA-TECDOC-1506, 2006 (unpublished).
[36] B. A. Brown, Phys. Rev. C **58**, 220 (1998).
[37] B. A. Brown, W. A. Richter, and R. Linsday, Phys. Lett. B **483**, 49 (2000).
[38] B. A. Brown, S. Typel, and W. A. Richter, Phys. Rev. C **65**, 014612 (2001).
[39] W. A. Richter and B. A. Brown, Phys. Rev. C **67**, 034317 (2003).
[40] J. Lee, J. A. Tostevin, B. A. Brown, F. Delaunay, W. G. Lynch, M. J. Saelim, and M. B. Tsang, Phys. Rev. C **73**, 044608 (2006).
[41] C. J. Batty *et al.*, Adv. Nucl. Phys. **19**, 1 (1989).
[42] H. W. Broek, T. H. Braid, J. L. Yntema, and B. Zeidman, Phys. Rev. **126**, 1514 (1962).
[43] U. Kiebele, E. Baumgartner, H. P. Gubler, H. O. Meyer, G. R. Plattner, and I. Sick, Helv. Phys. Acta **51**, 726 (1978).
[44] H. H. Chang, B. W. Ridley, T. H. Braid, T. W. Conlon, E. F. Gibson, and N. S. P. King, Nucl. Phys. A **270**, 413 (1976).
[45] A. Budzanowski *et al.*, Phys. Rev. C **17**, 951 (1978).
[46] G. Hauser, R. Löhken, H. Rebel, G. Schatz, G. W. Schweimer, and J. Specht, Nucl. Phys. A **128**, 81 (1969).
[47] D. A. Goldberg, S. M. Smith, H. G. Pugh, P. G. Roos, and N. S. Wall, Phys. Rev. C **7**, 1938 (1973).
[48] J. Albiński *et al.*, Nucl. Phys. A **445**, 477 (1985).
[49] Y. W. Lui, D. H. Youngblood, H. L. Clark, Y. Tokimoto, and B. John, Phys. Rev. C **73**, 014314 (2006).
[50] B. Bonin *et al.*, Nucl. Phys. A **445**, 381 (1985).
[51] M. Uchida *et al.*, Phys. Rev. C **69**, 051301(R) (2004).
[52] A. D. Dujcebaev, K. A. Kuterbekov, I. N. Kuhtina, B. M. Sadikov, L. I. Sliusarenko, V. V. Tokarevskii, and S. A. Faians, Joint Institute for Nuclear Research, Dubna Report No. JINR-P6-2001-223, 2001 (unpublished).
[53] H. L. Clark, D. H. Youngblood, and Y.-W. Lui, Phys. Rev. C **54**, 72 (1996).
[54] R. Perry, A. Nadasen, D. L. Hendrie, P. G. Roos, and N. S. Chant, Phys. Rev. C **24**, 1471 (1981).
[55] R. Tickle and W. S. Gray, Nucl. Phys. A **247**, 187 (1975).
[56] M. Takei, Y. Aoki, Y. Tagishi, and K. Yagi, Nucl. Phys. A **472**, 41 (1987).
[57] F. Hinterberger, G. Mairle, U. Schmidt-Rohr, G. J. Wagner, and P. Turek, Nucl. Phys. A **111**, 265 (1968).
[58] N. Matsuoka *et al.*, Nucl. Phys. A **455**, 413 (1986).
[59] E. J. Stephenson, J. C. Collins, C. C. Foster, D. L. Friesel, W. W. Jacobs, W. P. Jones, M. D. Kaitchuck, P. Schwandt, and W. W. Daehnick, Phys. Rev. C **28**, 134 (1983).

[60] A. C. Betker, C. A. Gagliardi, D. R. Semon, R. E. Tribble, H. M. Xu, and A. F. Zaruba, Phys. Rev. C **48**, 2085 (1993).
[61] C. Bäumer *et al.*, Phys. Rev. C **63**, 037601 (2001).
[62] N. Van Sen *et al.*, Phys. Lett. B **156**, 185 (1985).
[63] M. Ermer, H. Clement, G. Holetzke, W. Kabitzke, G. Graw, R. Hertenberger, H. Kader, F. Merz, and P. Schiemenz, Nucl. Phys. A **533**, 71 (1991).
[64] R. Röche, N. Van Sen, G. Perrin, J. C. Gondrand, A. Fiore, and H. Müller, Nucl. Phys. A **220**, 381 (1974).
[65] E. Newman, L. C. Becker, B. M. Preedom, and J. C. Hiebert, Nucl. Phys. A **100**, 225 (1967).
[66] A. Korff *et al.*, Phys. Rev. C **70**, 067601 (2004).
[67] J. Bojowald, H. Machner, H. Nann, W. Oelert, M. Rogge, and P. Turek, Phys. Rev. C **38**, 1153 (1988).
[68] G. Duhamel, L. Marcus, H. Langevin-Joliot, J. P. Didelez, P. Narboni, and C. Stephan, Nucl. Phys. A **174**, 485 (1971).
[69] H. Okamura *et al.*, Phys. Rev. C **58**, 2180 (1998).
[70] Experimental Nuclear Reaction Data (EXFOR / CSISRS), [http://www.nndc.bnl.gov/exfor/exfor00.htm].
[71] Computer codes JLM. JINA Special School on Methods of Direct Nuclear Reactions, Michigan State University, April 9–20, 2007; J. A. Tostevin (private communication).
[72] I. J. Thompson, Comput. Phys. Rep. **7**, 167 (1988).
[73] F. James and M. Roos, Comput. Phys. Commun. **10**, 343 (1975).
[74] W. W. Daehnick, J. D. Childs, and Z. Vrcelj, Phys. Rev. C **21**, 2253 (1980).
[75] H. X. An and C. H. Cai, Phys. Rev. C **73**, 054605 (2006).
[76] F. D. Becchetti Jr. and G. W. Greenlees, in *Polarization Phenomena in Nuclear Reactions*, edited by H. H. Barschall and W. Haeberli (The University of Wisconsin Press, Madison, WI, 1971), p. 682.
[77] X. Li, C. Liang, and C. H. Cai, Nucl. Phys. A **789**, 103 (2007).
[78] D. T. Khoa, G. R. Satchler, and W. von Oertzen, Phys. Rev. C **56**, 954 (1997).
[79] J. B. A. England, S. Baird, D. H. Newton, T. Picazo, E. C. Pollacco, G. J. Pyle, P. M. Rolph, J. Alabau, E. Casal, and A. Garcia, Nucl. Phys. A **388**, 573 (1982).
[80] M. Wit, J. Schiele, K. A. Eberhard, and J. P. Schiffer, Phys. Rev. C **12**, 1447 (1975).
[81] W. Karcz, I. Kluska, Z. Sanok, J. Szmider, J. Szymakowski, S. Wiktor, and R. Wolski, Acta Phys. Pol. B **3**, 525 (1972).
[82] H. R. Burgi, W. Gruebler, J. Nurzynski, V. Konig, P. A. Schmelzbach, R. Risler, B. Jenny, and R. A. Hardekopf, Nucl. Phys. A **321**, 445 (1979).
[83] G. Igo and B. D. Wilkins, Phys. Rev. **131**, 1251 (1963).
[84] A. Ingemarsson *et al.*, Nucl. Phys. A **676**, 3 (2000).
[85] A. Auce, R. F. Carlson, A. J. Cox, A. Ingemarsson, R. Johansson, P. U. Renberg, O. Sundberg, and G. Tibell, Phys. Rev. C **53**, 2919 (1996).
[86] K. Bearpark, W. R. Graham, and G. Jones, Nucl. Phys. **73**, 206 (1965).
[87] A. Budzanowski, L. Freindl, K. Grotowski, M. Rzeszutko, M. Słapa, J. Szmider, and P. E. Hodgson, Nucl. Phys. **49**, 144 (1963).
[88] H. Sakaguchi, M. Nakamura, K. Hatanaka, A. Goto, T. Noro, F. Ohtani, H. Sakamoto, and S. Kobayashi, Phys. Lett. B **89**, 40 (1979).
[89] H. Nishioka and R. C. Johnson, Phys. Rev. C **22**, 2457 (1980).
[90] P. J. Karol, Can. J. Chem. **61**, 750 (1983).